Journal of Catalysis 431 (2024) 115368

Contents lists available at ScienceDirect

Journal of Catalysis

journal homepage: www.elsevier.com/locate/jcat

Research article

Enhancing photocatalytic performance of atom transfer radical addition (ATRA) reactions in water using immobilized 10-Phenylphenothiazine catalysts on mesoporous silica supports

Montaña J. García [a], Thomas A. Comerford [b], Carmen Montoro [c,d], Eli Zysman-Colman [b,*], José Alemán [a,c,*], Silvia Cabrera [c,d,*]

[a] Organic Chemistry Department, Science Faculty, Universidad Autónoma de Madrid, 28049 Madrid, Spain
[b] Organic Semiconductor Centre, EaStCHEM School of Chemistry, University of St Andrews, Fife KY16 9ST, UK
[c] Institute for Advanced Research in Chemical Sciences (IAdChem), Universidad Autónoma de Madrid, 28049 Madrid, Spain
[d] Inorganic Chemistry Department, Science Faculty, Universidad Autónoma de Madrid, 28049 Madrid, Spain

ARTICLE INFO

Keywords:
Mesoporous silica materials
Heterogeneous catalysis
Photocatalysis
ATRA reactions

ABSTRACT

The development of catalysts is crucial for sustainable chemistry, and heterogeneous catalysis, specifically, can be environmentally friendly and recyclable. Catalyst immobilization in materials has been explored, in which mesoporous silica materials have shown outstanding results in catalysis. Photocatalysis has also gained attention, providing solutions for organic synthesis and late-state functionalization, mainly using homogeneous catalysts and organic solvents. The use of aqueous media for photocatalytic reactions is particularly attractive from a sustainability perspective yet can influence reaction chemoselectivity. However, poor solubility of the organic substrates and the catalyst limits photocatalytic methods in water. Mesoporous silicas are water-stable materials suitable for catalytic applications in such media, including photocatalysis. In this work, we demonstrate an atom transfer radical addition (ATRA) reaction in water using immobilized 10-phenylphenothiazine (PTH) catalyst on different mesoporous silica supports, showing improved photocatalytic performance compared to homogeneous conditions and substrate selectivity depending on the hydrophobicity of the alkene.

1. Introduction

The use of catalysts constitutes an important tool in the development of sustainable chemistry. Therefore, special attention has been paid to the development of catalysts, and in particular to heterogeneous catalysis because of its environmentally friendly and recyclable nature attributed to simple separation and recovery, as well as its applicability to continuous reactor operations. One of the approaches to the design of heterogeneous catalysts is its immobilization into material frameworks such as, carbon nanotubes [1], metal or covalent organic frameworks [2], among others [3]. Many different supports are available for this purpose but choosing the right one is crucial to confer the catalysts with not only the aforementioned sustainable characteristics of heterogeneous catalysts, but also incorporate extra features that permit an enhancement of their catalytic performance or that alter the expected selectivity of a transformation.

In the past few years, researchers in heterogeneous catalysis have drawn attention to the development of renewable approaches for technological processes such as biomass conversions and water treatment, and the use of the solar energy as energy source for CO_2 conversion, water splitting, and novel organic transformations, the progress of which relies heavily on the developments made in the field of photocatalysis [4]. However, water-mediated processes are challenging, mainly due to the impact of water on the stability and catalytic performance of the materials selected, and special emphasis should be placed on addressing catalyst deactivation, as well as ensuring the stability and structural integrity of the material in aqueous media [5]. Because of this, the development of water-compatible heterogeneous catalytic systems remains a major challenge, especially in the photocatalysis field.

Photocatalysis is considered a powerful tool in organic synthesis as it provides solutions not only for the construction of organic molecules but also for the chemoselective late-stage functionalization of complex molecules under mild reaction conditions [6]. In this field, the vast majority of examples use homogeneous photocatalysts, mainly

* Corresponding authors.
E-mail addresses: eli.zysman-colman@st-andrews.ac.uk (E. Zysman-Colman), jose.aleman@uam.es (J. Alemán), silvia.cabrera@uam.es (S. Cabrera).

https://doi.org/10.1016/j.jcat.2024.115368
Received 5 December 2023; Received in revised form 19 January 2024; Accepted 9 February 2024
Available online 15 February 2024

ruthenium(II) and iridium(III) complexes or organic dyes, and organic solvents [6]. The use of aqueous media for photocatalytic reactions has recently begun to be explored more extensively and these studies have revealed the different roles of water, ranging from serving as an electron donor to influencing the chemoselectivity of the reaction [7]. Although examples of the use of water as solvent for the development of photocatalytic transformations is scarce, such studies have demonstrated the stability and compatibility of common radical precursors, such as aryl bromides, carboxylic acids, etc., as well as the complexes in aqueous conditions [7]. However, the solubility of reagents and photocatalysts in water is generally poor and this limits the applicability of the photocatalytic methods in aqueous media.

Among the different water-stable materials, silicas, and more concretely, mesoporous silicas, stand out [8]. They have extraordinary stability and inertness against both water and organic solvents, and exceptional physicochemical properties [8]. For catalytic applications, the high surface area and tunable pores of mesoporous silica permit facile functionalization with the catalyst. To be more specific, the pores create a reaction pocket that can be customized in terms of its shape, size, and polarity. Additionally, the absence of visible-light absorption of the silica framework has been demonstrated to be optimal for developing photocatalytic materials, which resemble the photocatalytic properties of the parent catalyst [9].

In this context, the functionalization of alkenes and alkynes, both mono- and di-functionalization, plays an important role in organic chemistry. Its widespread application has sparked renewed interest in synthetic methodologies that employ clever strategies to efficiently construct complex molecules. Atom transfer radical addition (ATRA) reactions onto alkenes have emerged as influential tools with diverse applications in both industry and academic research, allowing the introduction of two functional groups into the double bond in a single operation step [10]. Building upon the groundbreaking work of Barton [11] and Stephenson [12], the most commonly utilized photoredox catalysts for ATRA processes have been ruthenium(II) or iridium(III) complexes, and more recently, homoleptic or heteroleptic copper complexes (approach, Fig. 1)[13]. However, the use of organic catalysts has been much less explored in this reaction, and to our knowledge the use of the 10-phenylphenothiazine (**Ph-PTH**) as a photocatalyst, recognized as particularly photoreducing ($E^{ox}_{1/2}{}^{*} = -2.1$ V vs. SCE) [14], has never been reported for this reaction. The use of such catalysts often presents challenges in terms of reusability and stability under photocatalytic conditions. Moreover, they tend to have low solubility in water, making them unsuitable for use in an aqueous environment. Previously, we had successfully immobilized platinum(II) catalysts onto mesoporous silica, observing confinement phenomena that resulted in a change in the photocatalytic activity.[15] In this work, we expand our immobilization technology to organic photocatalysts and investigate ATRA-type reactions in water using PTH immobilized on different mesoporous silica supports (approach b, Fig. 1). This approach offers several advantages, including enhanced stability of the photocatalyst, recyclability, and the potential for modified catalytic performance compared to homogeneous conditions.

2. Experimental section

2.1. Materials and methods

The description of all the materials, methods and instruments and full details of the experimental section are included in the Supporting Information (S.I.). **MSN**, [16] **SBA-15**, [17] their 3-aminopropyl derivatives, **MSN-AP** and **SBA-15-AP**, [15,18] PTH-CO_2H [19] and the starting alkenes **1b-1e** were synthesized following literature procedures and the synthesis is described in the S.I.. In this section, it is described a selection of the different procedures.

2.2. Synthesis of the heterogeneous photocatalysts MSN-AP-PTH and SBA-15-AP-PTH [20]

In the following procedure, the number of amino groups in **MSN-AP** or **SBA-15-AP** is calculated based on the %N of the elemental analysis and fixed as 1 equivalent.

In a round bottom flask, PTH-CO_2H [19] (1.0 equiv) was dissolved in *N,N*-dimethylformamide (DMF) (10 mL *per* 50 mg of silica). Then, 4-dimethylaminopyridine (DMAP, 3.1 equiv.) and *N*-(3-dimethylaminopropyl)-*N'*-ethylcarbodiimide hydrochloride (EDC, 3.4 equiv.) were added, and the reaction mixture was stirred for 15 min at room temperature. Finally, the corresponding **MSN-AP** or **SBA-15-AP** (1.0 equiv.) was added, and the reaction was stirred for 24 h. A grey-pale solid was formed which was isolated by centrifugation and washed with DMF (3 × 30 mL), ethyl acetate (EtOAc) (3 × 30 mL) and diethyl ether (Et_2O) (3

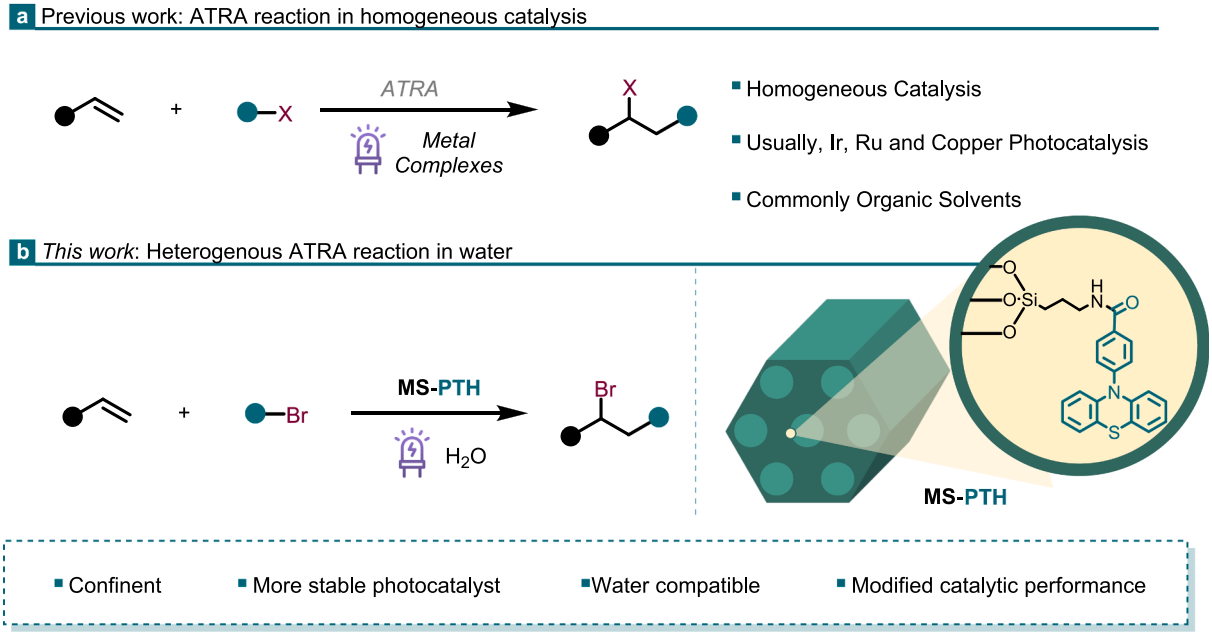

Fig. 1. Context of the ATRA reaction and present work with MS-PTH material.

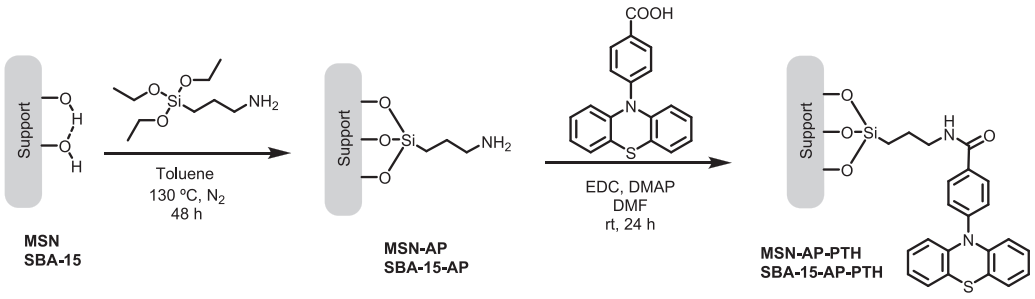

Scheme 1. Synthesis of **MSN-AP-PTH** and **SBA-15-AP-PTH** materials.

× 30 mL). The **MSN-AP-PTH** and **SBA-15-AP-PTH** materials were dried under vacuum overnight.

2.3. Synthesis of N-butyl-4-(10H-phenothiazin-10-yl)benzamide PTH-CONH-Bu

In a round bottom flask, PTH-CO_2H [19] (64.3 mg, 0.2 mmol) was dissolved in 4.0 mL of dichloromethane (DCM). Then, oxalyl chloride (17.0 µL, 0.2 mmol,) and a drop of DMF were added. This mixture was stirred at reflux for 4 h. Then, the solvents were evaporated, and the crude mixture was diluted with 4 mL of DCM. Next, triethylamine (Et_3N) (60 µL, 0.4 mmol) and butylamine (59.3 µL, 0.6 mmol) were added and the reaction was stirred for 16 h. The catalyst was obtained pure after column chromatography purification (silica gel, Cyhex:EtOAc 4:1) in a 60 % yield (44.5 mg, pale-white solid).

^{1}H NMR (300 MHz, $CDCl_3$): δ 7.89 (d, J = 8.0 Hz, 2H), 7.33 (d, J = 8.0 Hz, 2H), 7.18 – 7.10 (m, 2H), 6.95 (dq, J = 13.2, 7.1 Hz, 4H), 6.50 (d, J = 7.7 Hz, 2H), 6.31 (bs, 1H), 3.48 (q, J = 6.7 Hz, 2H), 1.70 – 1.54 (m, 2H), 1.49 – 1.35 (m, 2H), 0.97 (t, J = 7.2 Hz, 3H). ^{13}C NMR (75 MHz, $CDCl_3$): δ 166.8, 145.1, 143.2, 132.6, 129.1, 127.4, 127.0, 126.7, 124.2, 123.7, 119.1, 39.9, 31.8, 20.2, 13.8. HRMS (ESI$^+$): Calculated for $C_{23}H_{23}N_2OS$ $[M + H]^+$: 375.1531, found: 375.1458.

2.4. General procedure for the photocatalytic ATRA reaction

In a 10.0 mL vial charged with a stirring bar, the corresponding alkene **1a-1e** (0.1 mmol), 2-bromoacetophenone (**2**) (24.0 mg, 0.12 mmol), LiBr (8.7 mg, 0.1 mmol), **MSN-AP-PTH** (0.6 mol% of PTH) and 300 µL of water were added. Then, the vial was sealed with a PTFE/rubber septum and three freeze pump-thaw cycles were applied. The reaction mixture was stirred under 420 nm irradiation at 20.0 °C for the corresponding time. The crude reactions were analysed by ^{1}H NMR. For that, 2.8 mg of 1,3,5-trimethoxybenzene (6.1 ppm, 3H; 3.8 ppm, 9H) as internal standard and 0.5 mL of $CDCl_3$ were added to the reaction mixture, which was shaken.

2.5. Catalyst recycling

Once the photocatalytic ATRA reaction was completed and analysed by ^{1}H NMR, the reaction mixture was centrifuged (2 × 5 min at 10000 rpm), and the supernatant was removed. Then, the material was washed with DCM (3 × 10 mL), acetone (1 × 10 mL) and Et_2O (3 × 10 mL) and dried. Next, the material was collected in a vial for being used in the next cycle by addition of a new batch of fresh reagents for undergoing the general procedure of the ATRA reaction. This procedure was repeated for each photocatalytic cycle.

3. Results and discussion

3.1. Synthesis and characterization of the materials

The synthesis of the desired photocatalytic materials **MSN-AP-PTH** and **SBA-15-PTH** was planned via post-functionalization of the corresponding aminopropyl-functionalized silica (**MSN-AP** or **SBA-15-AP**) with the carboxylic acid derivative of the PTH (PTH-CO_2H) (Scheme 1) [19]. Previously, the aminopropylated silicas were prepared by stirring **MSN** or **SBA-15** in toluene at reflux with (3-aminopropyl)triethoxysilane (APTS) following reported procedures [15,18]. The successful functionalization of the silicas with the AP groups was corroborated by IR analysis of the **MSN-AP** and **SBA-15-AP** samples, which presented the characteristic N–H and C–H stretching vibration bands at ~ 3000 cm^{-1} (see S.I.). The incorporation of the aminopropyl groups to the silica allowed for the covalent anchoring of the photocatalyst into the material through an amide bond. Thus, the coupling of PTH-CO_2H with the two different amino-functionalized silicas was conducted in the presence of DMAP and EDC. To optimize the conditions of this transformation it was key to previously quantify the number of amino groups of the aminopropylated silicas (**MSN-AP** or **SBA-15-AP**) by elemental analysis.

For comparative purposes, we have also prepared the *N*-butylamide derivative of the PTH photocatalyst (**PTH-CONHBu**), starting from PTH-CO_2H (Scheme 2). We consider **PTH-CONHBu** as the homogeneous

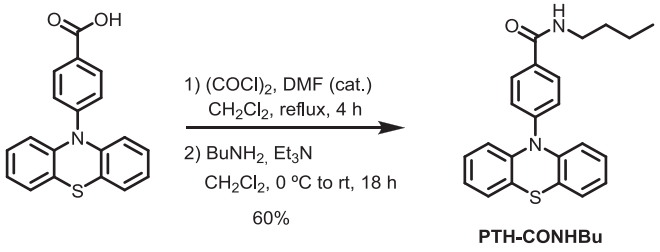

Scheme 2. Synthesis of **PTH-CONHBu** compound.

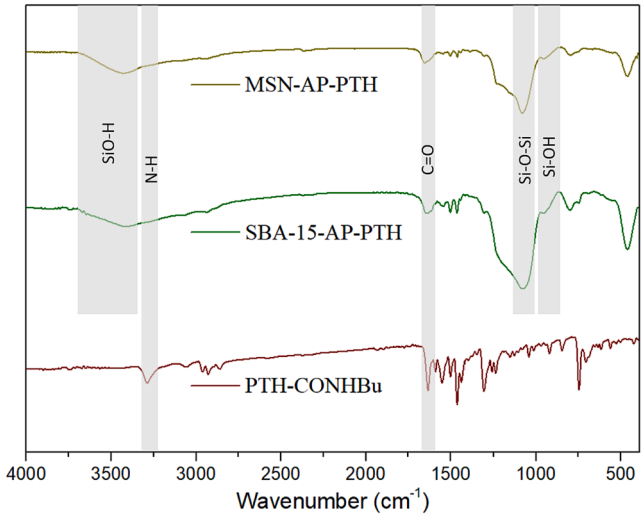

Fig. 2. IR spectra of **MSN-AP-PTH** and **SBA-15-AP-PTH** materials, and homogeneous **PTH-CONHBu.**

Table 1
Main physico-chemical parameters of **MSN-AP-PTH, SBA-15-AP-PTH** and the parent silica materials.

Material	Pore size (Å)	BET ($m^2 \cdot g^{-1}$)[a]	Total volume ($cm^3 \cdot g^{-1}$)	S content (% w/w)[b]	PTH content ($mmol \cdot g^{-1}$)[c]
MSN-AP	45.0	363	0.61	–	–
MSN-AP-PTH	25.0	100	0.43	1.250	0.389
SBA-15-AP	35.0	265	0.28	–	–
SBA-15-AP-PTH	30.0	97	0.11	0.435	0.136

[a] BET: specific surface area calculated from the nitrogen physisorption data.
[b] Determined by CHNS elemental analysis.
[c] Calculated according to the S content.

photocatalyst electronically equivalent of the supported ones (**MSN-AP-PTH** and **SBA-15-AP-PTH)**. Firstly, PTH-CO_2H was converted into its corresponding acyl chloride using oxalyl chloride, which was subsequently reacted with butylamine to afford **PTH-CONHBu** in a 60 % of overall yield.

The heterogeneous photocatalysts **MSN-AP-PTH** and **SBA-15-AP-PTH** were fully characterized. The analysis and comparison of the IR spectra, in particular the amide carbonyl stretching vibration at 1640 cm^{-1}, of both functionalized materials with that of the parent aminopropyl-silica and the homogeneous **PTH-CONHBu** confirmed the adequate binding of the photocatalyst to the amino group of the corresponding **MSN-AP** or **SBA-15-AP** silica (Fig. 2 and S.I.). The disappearance of the strong stretching band of the COO-H indicated that no free PTH-CO_2H photocatalyst was present inside the pores; additionally, the corresponding stretching bands of the silica framework (Si-OH and Si-O-Si) were also observed in the **MSN-AP-PTH** and **SBA-15-AP-PTH** spectra.

Both **MSN** and **SBA-15** are mesoporous silicas having the same chemical composition but with some differences (Table 1). They both have a hexagonal arrangement of their pores, but those of **MSN** are smaller than those of **SBA-15**. On another hand, **SBA-15** particles are elongated spheres of less than 700 nm whereas **MSN** are spheres of ~ 80 nm of diameter [16,17]. Such morphology and pore arrangement were maintained after the functionalization of the silicas with PTH as indicated in the SEM and TEM images of **MSN-AP-PTH** and **SBA-15-AP-PTH** samples (Fig. 3).

The mesoscopic structure of the PTH-modified silica materials was identified by powder X-ray diffraction (XRD) and compared to that of the parent **MSN** and **SBA-15** silicas. As shown in Fig. 4, the functionalization of the silicas with PTH did not result in any displacement of the Miller peaks corresponding to the hexagonal mesoscopic order. However, a noticeable decrease in their intensity was observed, which indicates the presence of the PTH within the pores [21]. Those data are also in agreement with the textural properties of the materials determined by the measurements of their N_2 adsorption–desorption isotherms at −196 °C (Table 1 and Fig. 5). As expected, there is a decrease in the surface area, the total volume, and diameter of the pores after the functionalization of **SBA-15-AP** and **MSN-AP** with PTH due to the limitation in diffusion and the reduction of the pore sizes. This fact confirms the incorporation of the PTH catalyst inside the pores.

SBA-15-AP and **SBA-15-AP-PTH** present a type IV isotherm (Fig. 5a-b) according to the IUPAC classification [22]. This kind of isotherm is

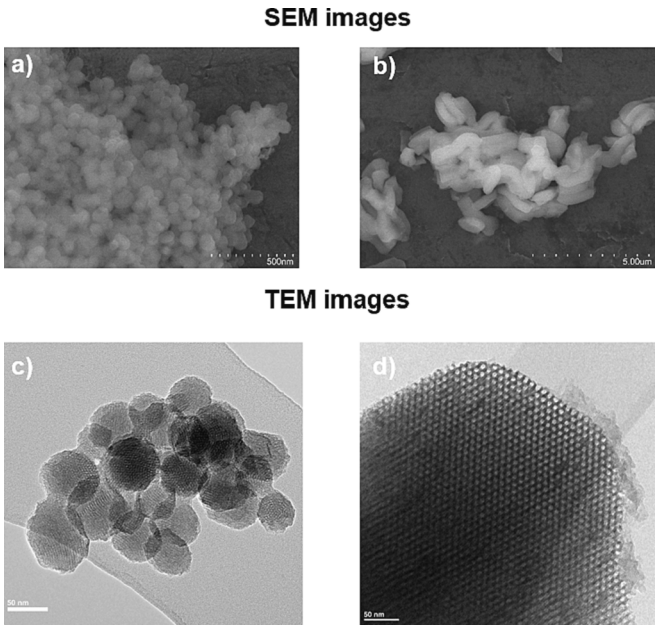

Fig. 3. SEM and TEM images of **MSN-AP-PTH** (a and c), and **SBA-15-AP-PTH** (b and d) materials.

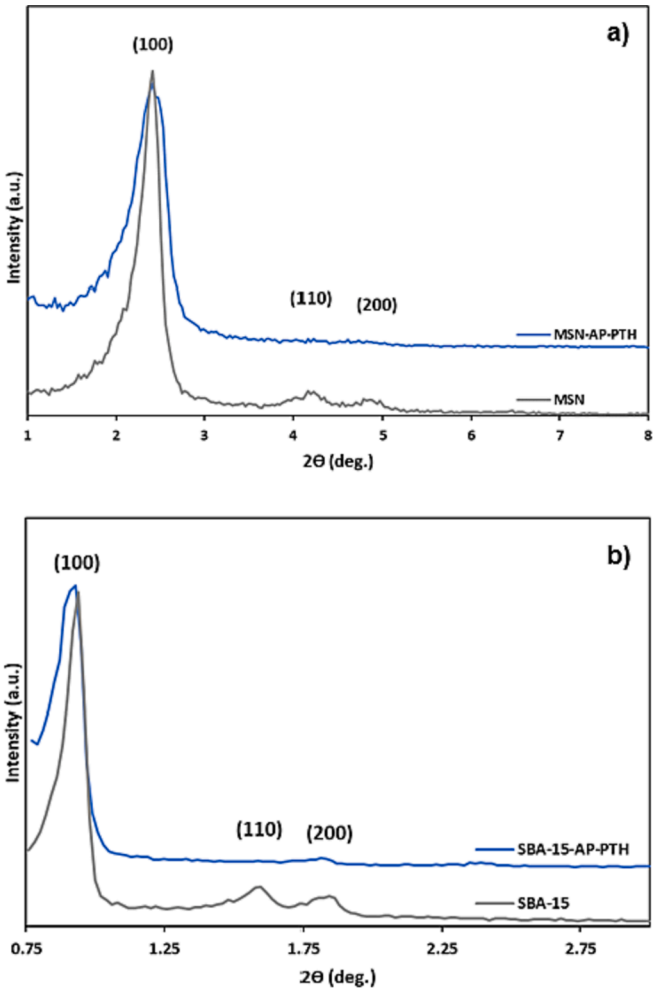

Fig. 4. Powder XRD patterns of a) non-functionalized **MSN** and **MSN-AP-PTH**, and b) non-functionalized **SBA** and **SBA-15-AP-PTH**.

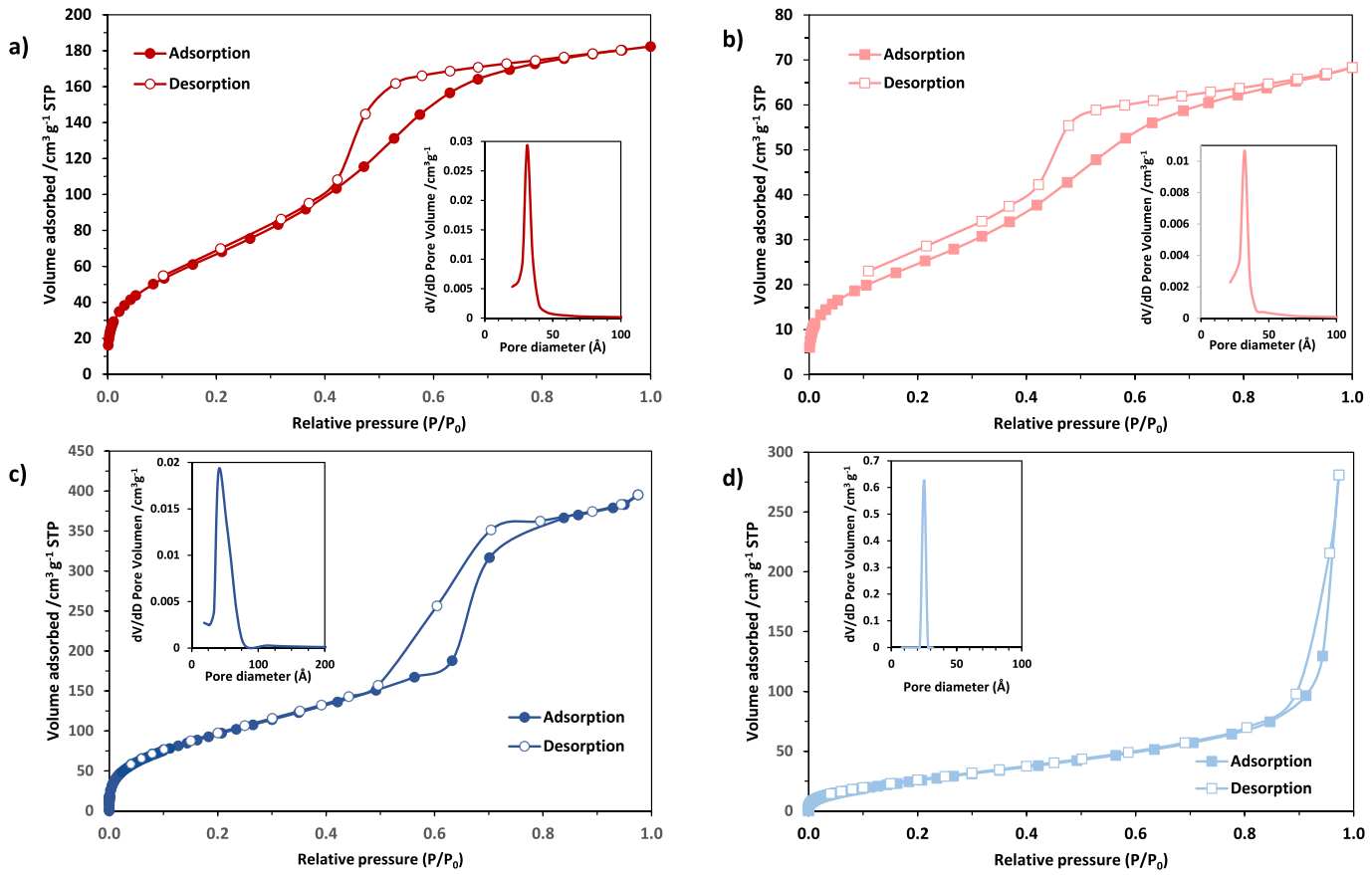

Fig. 5. Nitrogen adsorption–desorption isotherms and pore size distribution curves for a) **SBA-15-AP**, b) **SBA-15-AP-PTH,** c) **MSN-AP** and d) **MSN-AP-PTH**.

characterized by an H1 hysteresis loop due to the capillary condensation that occurs in mesoporous materials with cylindrical pores [23]. The BJH analysis of the nitrogen desorption data reveals a well-defined pore-size distribution with narrow peaks and an average pore size of 35 and 30 Å for **SBA-15-AP** and **SBA-15-AP-PTH**, respectively. These findings strongly suggest that both materials maintain a consistent and uniform mesopore size. **MSN-AP** exhibits isotherms between type IV and type VI (Fig. 5c), emphasizing its mesoporous nature [22]. Furthermore, this isotherm shows a hysteresis loop, occurring between P/P_0 0.8 and approximately 0.5. This loop is a result of the capillary condensation of nitrogen into the straight pores of the system [24]. On the other hand, the isotherm of **MSN-AP-PTH** is type III (Fig. 5d), which is characteristic of nanoporous or non-porous materials [22]. Indeed, the **MSN-AP** and **MSN-AP-PTH** BET surface areas decreases from 363 to 100 $m^2 \cdot g^{-1}$, respectively, due to the functionalization (Table 1). Likewise, the pore size changes from 45 to 25 Å, which confirms the presence of PTH inside the pores.

Finally, the amount of PTH bound to the silica materials was calculated according to the sulfur (S) content determined by elemental analysis (Table 1). For sample **MSN-AP-PTH**, a 1.25 % wt. of S was found, which corresponds to 0.389 mmol of PTH per gram of silica. By contrast, the loading of PTH within the SBA-15 material was lower, being 0.136 mmol of PTH per gram of SBA-15 (based on 0.435 % of S).

3.2. Photophysical properties

Attempts at forming stable suspensions of the molecular catalysts and their supported counterparts were made in each of ethanol (EtOH), tetrahydrofuran (THF), and methanol (MeOH). Those in MeOH formed sufficiently stable suspensions for photophysical measurements to be caried out and MeOH was therefore chosen as the solvent for the

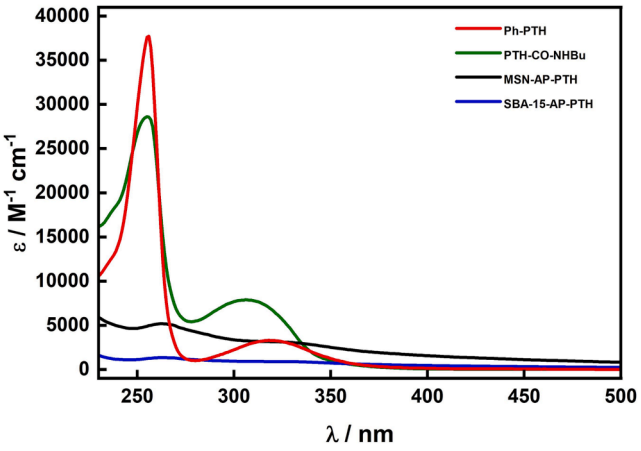

Fig. 6. Molar extinction coefficients for **Ph-PTH** and the three PTH-based photocatalysts in MeOH.

photophysical measurements. The absorption spectra of the molecular **PTH-CONHBu** and heterogeneous **MSN-AP-PTH** and **SBA-15-AP-PTH** materials were compared with their structural parent, **Ph-PTH** (Fig. 6). The absorption spectra of **Ph-PTH** and **PTH-CONHBu** in MeOH are similar, both having bands centered at around 255 nm and both having a second, lower intensity band at around 310 and 325 nm, respectively. The absorption spectra of the two mesoporous silica species reveal that the high-energy band is much less intense, appearing at around ~ 270 nm. Of particular interest is the long absorption tail out to 500 nm. The most highly absorbing species at 420 nm, the excitation wavelength used for the photocatalysis, is **MSN-AP-PTH** with an $\varepsilon_{420\ nm}$ = ~1500

$M^{-1}{\cdot}cm^{-1}$, significantly higher than seen for **SBA-15-AP-PTH** with $\varepsilon_{420\ nm}$ = ~500 $M^{-1}{\cdot}cm^{-1}$. Both molecular species, **Ph-PTH** and **PTH-CONHBu**, absorb far less than their silica counterparts at this wavelength, with **Ph-PTH** $\varepsilon_{420\ nm}$ ~ 100 $M^{-1}{\cdot}cm^{-1}$ and **PTH-CONHBu** showing negligible absorption at 420 nm.

Upon measuring the emission spectra of these compounds in MeOH (λ_{exc} = 420 nm) it was found that only **PTH-CONHBu** was emissive, showing a main broad band at 520 nm (see S.I., Figure S27). The emission spectra in THF and toluene are similar but the broad band blue-shifts with decreasing polarity, thus permitting us to assign this emission to originating from a charge-transfer state.

The time-resolved photoluminescence decay of **Ph-PTH** showed mono-exponential decay kinetics with a lifetime of τ_{PL} = 2.6 ns (Fig. 7a), while that of **PTH-CONHBu** displayed a biexponential lifetime under vacuum of τ_{PL} = 0.4 ns (10 %), 12 ns (90 %), which remains similar upon aeration with biexponential lifetime τ_{PL} = 0.4 ns (9 %), 8.8 ns (91 %) (Fig. 7b). Despite the very poorly emissive nature of the **MSN-AP-PTH,** the lifetime studies revealed the emission intensity was oxygen sensitive (Fig. 7c). The degassed solution has a lifetime of τ_{PL} = 2.43 μs, but upon aeration this lifetime decreases to 838 ns. This would suggest that this material shows very weak room temperature phosphorescence (RTP). Indeed, derivatives of phenothiazine have been previously reported to show RTP [25]. **SBA-15-AP-PTH** on the other hand showed no long-lived emission or sensitivity towards oxygen. The weak emission of this sample decays with triexponential kinetics that do not change in the presence of oxygen (τ_{PL} under vacuum = 1.4 ns (42 %), 4.3 ns (49 %), and 12.9 ns (9 %), and τ_{PL} under air = 1.5 ns (58 %), 4.2 ns (37 %), and 11.8 ns (6 %) (Fig. 7d). The difference in behaviour in the time-resolved PL between these two samples may be due to the different conformations of the dye, which can adopt both a planar and a puckered conformation of the phenothiazine. In the confined silica networks the conformational landscape may be different in these two materials, thus explaining the difference in the observed behaviour [26].

3.3. Catalytic activity

To evaluate the catalytic activity of **MSN-AP-PTH** and **SBA-15-AP-PTH**, we chose the ATRA of activated bromoalkanes to alkenes as a model reaction [11–13]. Even though this transformation can be considered as an atom-economic difunctionalization of olefinic substrates, we nonetheless wanted to develop an improved version by using a heterogeneous photocatalyst and water as a green solvent. To achieve this goal, we first tested the activity of **SBA-15-AP-PTH** in the radical addition of 2-bromoacetophenone (**2**) to 5-hexen-1-ol (**1a**) in the presence of LiBr using water as solvent and irradiating at 420 nm, based on previous ATRA reaction conditions [11–13] (Table 2). Under these conditions, only 0.6 mol% of PTH anchored to SBA-15 silica was found to efficiently catalyse the ATRA reaction under study (Table 2, entry 1). Surprisingly, increasing the catalytic loading of **SBA-15-AP-PTH** to 1 mol% produced a sluggish reaction and the yield of product **3a**

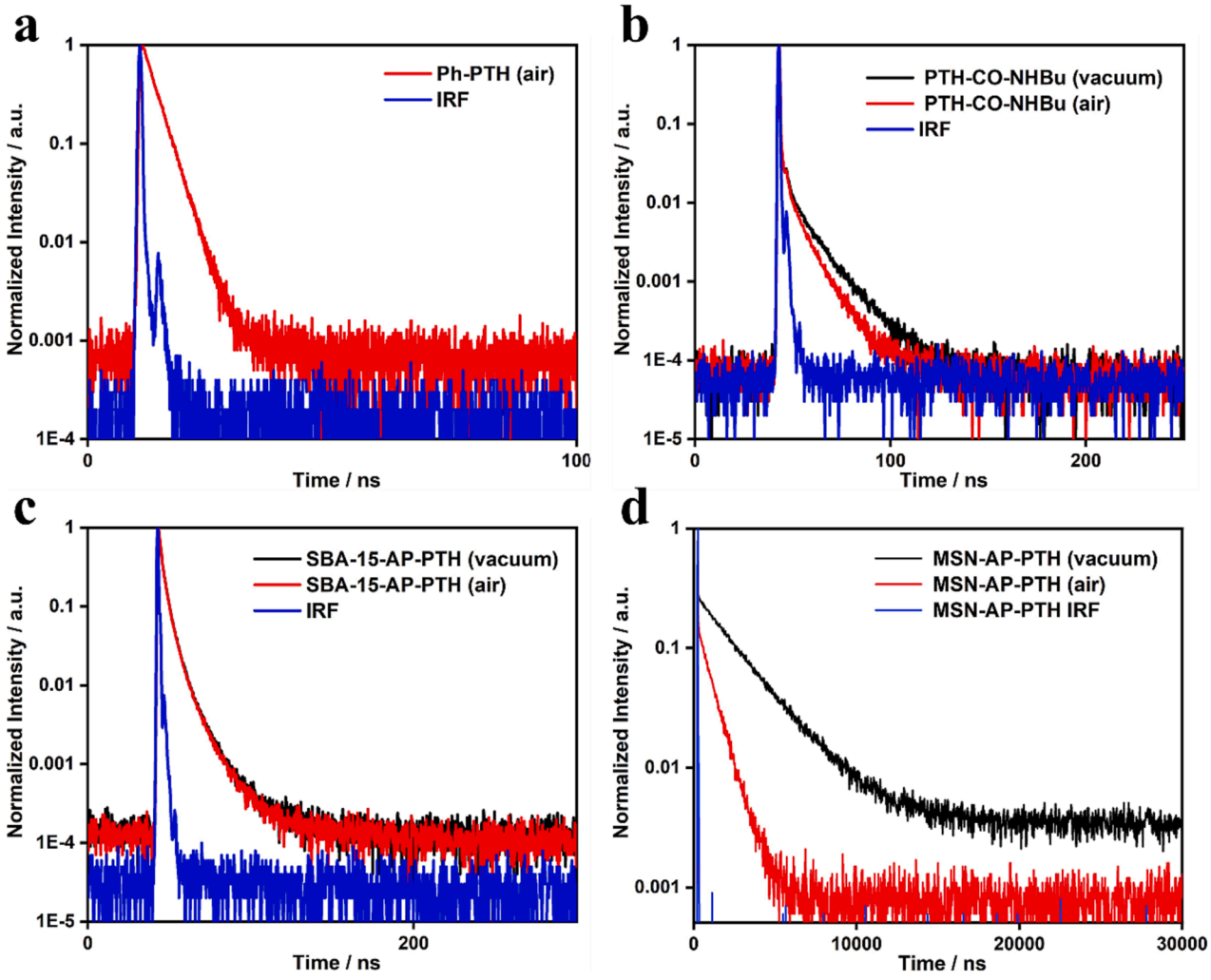

Fig. 7. Time-resolved PL decays of a) **Ph-PTH**, b) **PTH-CONHBu**, c) **MSN-AP-PTH**, d) **SBA-15-AP-PTH**. All spectra were measured in MeOH. λ_{exc} = 375 nm. IRF denotes the Instrument Response Function.

Table 2
ATRA reaction of alkene **1a** with **2** catalyzed **SBA-15-AP-PTH** [a].

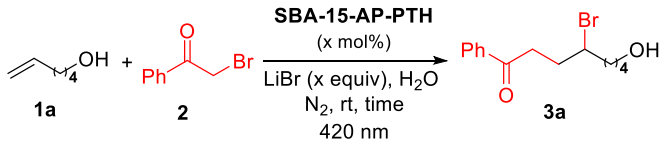

Entry	**SBA-15-AP-PTH** (mol% PTH)	LiBr (x equiv.)	Variations[a]	Yield (%)[b]
1	0.6	1	–	70
2	1	1	–	42
3	0.6	2	–	56
4	0.6	–	–	50
5	0.6	1	0.6 mL H_2O	35
6	0.6	1	No light	n.r.
7	0.6	1	Under O_2	n.r.
8	–	1	–	9
9	–	1	using **SBA-15** or **SBA-15-AP**	8

[a] Reaction conditions: A mixture of **1a** (0.1 mmol), **2** (0.12 mmol), LiBr (1–2 equiv) and **SBA-15-AP-PTH** (0.6–1 mol% of PTH) in water (0.3 mL) was irradiated at 420 nm under nitrogen atmosphere during 4 h. [b] ^{1}H NMR yield calculated from the reaction mixture using 1,3,5-trimethoxybenzene as internal standard. n.r. denotes no reaction.

Table 3
Model ATRA reaction using different heterogeneous silicas as photocatalysts [a].

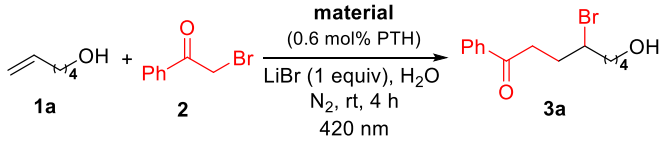

Entry	Material	Pore size (Å)	Yield (%)[b]
1	**SBA-15-AP-PTH**	30.0	70
2	**MSN-AP-PTH**	25.0	97

[a] Reaction conditions: A mixture of **1a** (0.1 mmol), **2** (0.12 mmol), LiBr (1 equiv) and **SBA-15-AP-PTH** or **MSN-AP-PTH** (0.6 mol% of PTH) in water (0.3 mL) was irradiated at 420 nm under nitrogen atmosphere during 4 h. [b] ^{1}H NMR yield calculated from the reaction mixture using 1,3,5-trimethoxybenzene as internal standard.

diminished (Table 2, entry 2). Next, we evaluated the effect of the amount of LiBr has on the reaction outcome, determining that 1 equivalent was the optimal amount to achieve high yields (Table 2, entries 1, 3–4). Finally, the concentration of the reaction mixture was studied as well. The results showed that concentration is another critical parameter among the reaction conditions and the best catalytic performance was obtained using 0.3 mL of water instead of 0.6 mL (Table 2, entries 1, 5). We note that the reaction does not occur in the absence of light, catalyst, nor in the presence of oxygen (Table 2, entries 6–8), and **SBA-15** and **SBA-15-AP** silicas that are catalyst-free are also not able to catalyse the reaction (Table 2, entry 9).

With the optimized conditions in hand, we next evaluated the two catalytic materials prepared (**MSN-AP-PTH** and **SBA-15-AP-PTH**) in the model transformation. As can be observed in Table 3, this comparative study documented the catalytic outperformance of **MSN-AP-PTH** over **SBA-15-AP-PTH** (97 % vs 70 % yield), [27] even though both experiments were performed using the same amount of the photocatalyst loading (0.6 mol% of PTH) and reaction conditions. It is well-known that the size and morphology of the particles and the pore size of the silicas affect their catalytic activity [15,28]. Here, we could attribute the superior photocatalytic performance of PTH within the MSN silica to the nanoenvironment provided by the smaller confined space in the MSN silica (25.0 Å of pore size), compared to that of SBA-15 (30.0 Å of pore size), which seems to favour the interaction between the reactants within the pore space and consequently, the reaction efficiency.

One important feature of mesoporous silica is their ability to modulate the activity of the embedded catalyst. Reported studies have described how the pore size of those materials and the polarity of the environment surrounding the anchored catalyst can modulate (enhance or inhibit) their activity [15,29]. To investigate this feature, we tested **MSN-AP-PTH** in the ATRA reaction using alkenes having substituents proximal to the alcohol moiety (**1**) with different steric, hydrogen bonding, and polar characteristics.[30] Thus, in addition to the previously examined alkene **1a** containing a primary hydroxyl group, alkenes substituted with *N*-Boc- and *N*-Fmoc-glycinate (**1b** and **1c**, respectively), diethylphosphate (**1d**) and methylsulfonate (**1e**) were submitted to the photocatalytic ATRA conditions under **MSN-AP-PTH** catalysis. Table 4 shows the yields of the corresponding product **3** obtained after 4 h of reaction. The first data extracted from these results are the higher ATRA reaction yield in the case of the unsubstituted alcohol **1a**, obtaining a 97 % of product **3a** after 4 h. Regarding substituted compounds **1b-1e**, different reaction progressions were obtained depending on the compound studied. Considering that in all the experiments, the photocatalytic conditions and the silica material are the same, but the only significant difference is the hydroxyl protecting group of **1** which does not participate in the ATRA mechanism, it is difficult to reconcile the differences in the yields found for the substrates **1b-1e**. First, to clarify if these differences are due to the intrinsic properties of **MSN-AP-PTH** or of those of the alkenes, we also performed the ATRA reaction of compounds **1a-1e** using the homogeneous **PTH-CONHBu** photocatalyst (Table 4). This comparative study was performed using 0.6 mol% of photocatalyst in both the silica material and as the molecular catalyst. First, the outstanding catalytic performance of **MSN-AP-PTH** towards the ATRA reaction of the free alkenol **1a** was confirmed, surpassing the

Table 4
Experimental yield of product **3** under catalytic **MSN-AP-PTH** material and homogeneous **PTH-CONHBu**, and physicochemical parameters of alkenes **1a-1e**.

Alkene **1**	Yield (%)[a]		Molecule size (Å^2)[b]	logP[c]	logS[c]
	using **MSN-AP-PTH**	using **PTH-CONHBu**			
1a (OH)	97	74	9.14 × 2.97	1.30	−0.94
1b (Boc-Gly)	50	100	17.29 × 4.38	2.36	−3.07
1c (Fmoc-Gly)	20	60	21.30 × 8.76	4.42	−5.91
1d ($PO(OEt)_2$)	67	88	12.80 × 8.39	2.10	−1.64
1e (SO_2Me)	91	80	11.30 × 2.74	1.51	−2.40

[a] Yield of product **3** calculated using ^{1}H NMR (see S.I.). [b] The size of each molecule was calculated multiplying the length of the molecule by the width. These values were measured with Chem3D program after MM2 geometry optimization. [c] Estimated logP and logS values obtained with the ALOGPS 2.1 program (https://www.vcclab.org/lab/alogps/).

reactivity obtained using the homogeneous **PTH-CONHBu** catalyst. However, the molecular catalyst is generally more effective than the anchored one for the ATRA reaction of O-substituted alkenes **1b-1d**. Moreover, there is no clear trend that could be discerned between the reactivity found using the homogeneous or heterogeneous catalytic systems. These changes in the reactivity should be examined considering that the catalytic reaction under the homogeneous catalysis takes places in an open space whereas the reaction catalysed by **MSN-AP-PTH** undergoes in a confined space in addition to a different polarity environment. This nanoreactor space is constituted of the Si-O-Si walls, the hydrophobic catalyst and the pore of the silica contain mainly propylamino groups, and rarely silanol groups due to the high-temperature

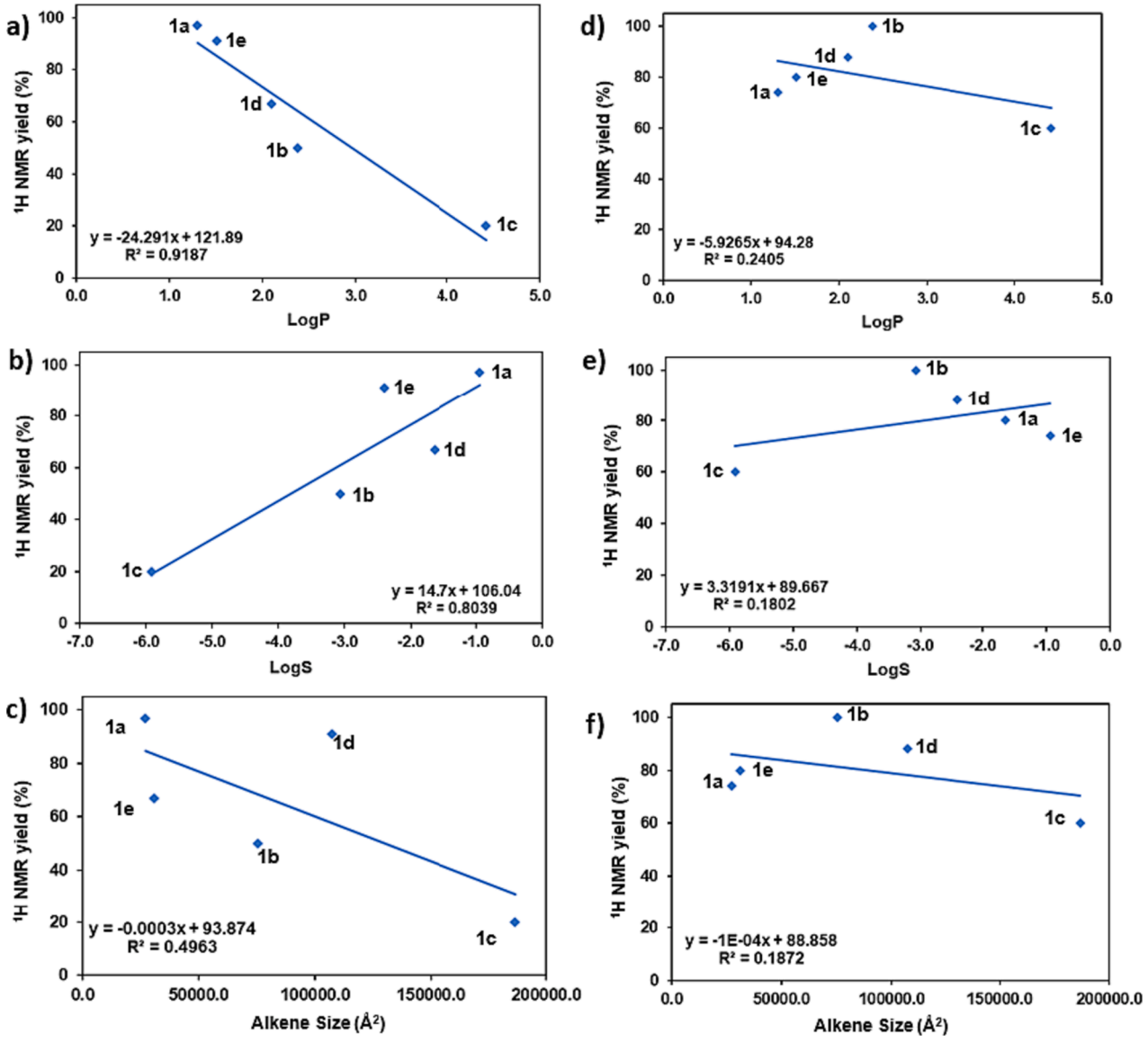

Fig. 8. Relationships between the experimental yield obtained for the substrates **1** after 4 h of reaction and a) log P, b) logS, c) molecule size of alkene **1** under catalytic **MSN-AP-PTH** material; and d) log P, e) logS, f) molecule size of alkene **1** under homogeneous **PTH-CONHBu**.

grafting methods that ensures a high functionalization degree. All these features create a hydrophobic environment around the photocatalyst that would be expected to modify the photophysics and thus the performance of the catalyst. In fact, as previously commented, both materials and the molecular photocatalyst present differences in the time-resolved PL decays and lifetimes. Moreover, it has also been reported that the morphological properties of the mesoporous silica materials influence the reaction outcome of different organic transformations [31]. For example, the size of the pores can control the diffusion rates of reactants and products, and as a result, different product selectivities are possible.

To clarify the origins of the reactivity observed with **MSN-AP-PTH**, we analysed different parameters such as the hydrophobicity, solubility, and the size of the akenes **1** (Table 4). The hydrophobicity of the substrates was estimated using the *n*-octanol–water partition coefficient, expressed as logP, which was calculated using the ALOGPS 2.1 program. Moreover, the same program allowed to calculate the solubility of alkenes **1a-1e** as logS values. For estimating the size of alkenes **1**, we have estimated it based on the height and width of each molecule measured using Chem3D after the geometry optimization.

The relationship between such parameters and reaction yields using **MSN-AP-PTH** was investigated using graphical representation (Fig. 8a-c and Table 4). A parallel analysis was performed with the reaction yields obtained under the homogeneous photocatalyst conditions using **PTH-CONHBu** (Fig. 8d-f and Table 4). Upon initial analysis of the graphs depicting reactions conducted under homogeneous catalyst **PTH-CONHBu** (Fig. 8d-f), no correlation was observed between any of the parameters studied (molecule size, solubility, and hydrophobicity of alkene **1**) and the reaction outcome. Conversely, the ATRA reaction catalysed by **MSN-AP-PTH** showed a linear relationship between hydrophobicity (logP) and the yield of product **2** (Fig. 8a). As well, there is a correlation between the solubility of alkene **1** (logS) and the reaction yield (Fig. 8b). Finally, the size of the alkene **1** seems to have no influence in the reaction yield (Fig. 8c). These results evidence that the hydrophobicity of the alkene is the main factor influencing the photocatalytic performance of **MSN-AP-PTH**. Thus, the less hydrophobic the molecule (lower logP), the higher is their reaction yield towards the ATRA reaction catalysed by **MSN-AP-PTH.**

Finally, the robustness and recyclability of **MSN-AP-PTH** was assessed in the ATRA reaction between **2** and **1a**. For this purpose, when the reaction reached full conversion, the catalyst was separated from the reaction mixture by centrifugation, washed and dried. Then, **MSN-AP-PTH** was submitted to a new catalytic cycle by adding a fresh set of reagents and solvent. Following such a recycling sequence, **MSN-AP-PTH** was able to maintain the catalytic activity across 4 runs (Fig. 9), demonstrating the recyclability of the catalyst. In addition, the potential for catalyst leaching was evaluated through hot filtration of the reaction mixture. Thus, after a certain conversion level the reaction mixture was filtrated for removal of the catalyst and the reaction mixture was allowed to proceed for an additional time. Following this procedure, we performed the filtration at 80 % conversion level. After the removal of the catalyst, the ATRA reaction was stopped, suggesting that there are no soluble catalytic species present in the reaction medium and that only the anchored PTH catalyst is responsible for the catalytic activity observed in the material. Finally, the recovered photocatalyst **MSN-AP-PTH** was characterized by elemental analysis and IR (see Figure S3 and Table S2, S.I.). Both techniques showed that the chemical integrity of the material was preserved after the catalytic run. Furthermore, the maintenance of the morphology of the material after the reaction was confirmed by SEM (see Figure S3, S.I.). The results of these experiments demonstrated the excellent stability and recyclability of the **MSN-AP-PTH** photocatalyst in the reaction under investigation.

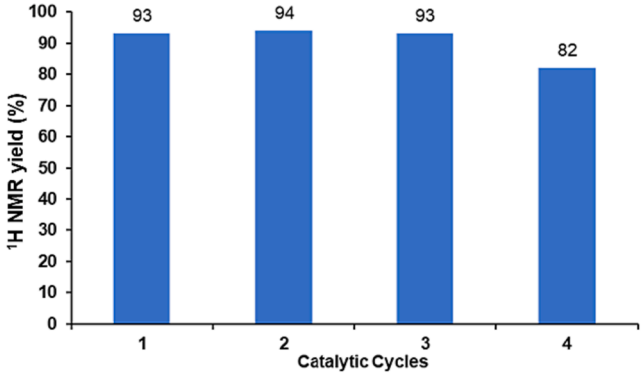

Fig. 9. Variation of yield of product **3a** with the number of catalytic cycles using **MSN-AP-PTH** material.

4. Conclusions

In this work, we described the evaluation of two photocatalyst materials, **MSN-AP-PTH** and **SBA-15-AP-PTH**, for the ATRA reaction of alkenes. The catalytic activity of **MSN-AP-PTH** was found to be superior to that of **SBA-15-AP-PTH** under the same reaction conditions and catalyst loading. The higher photocatalytic performance of PTH within MSN silica compared to SBA-15 may be attributed to the smaller confined space provided by MSN silica and its better photophysical properties, namely a higher absorption at 420 nm and longer-lived excited state in the microsecond regime under the degassed conditions used in photocatalysis. This confined space favours the interaction between reactants, leading to increased reaction yields. We have also studied the ATRA reaction using different alkenes with various substituents at the alcohol moiety. The reactivity and yields varied depending on the substrate. It was observed that the hydrophobicity of the alkene played a significant role in the photocatalytic performance of **MSN-AP-PTH**. Thus, the use of less hydrophobic alkenes led to higher reaction yields. In addition, the recyclability and stability of **MSN-AP-PTH** catalyst were demonstrated. The catalyst maintained its activity during four reaction cycles, and there was no evidence of catalyst leaching or degradation.

CRediT authorship contribution statement

Montaña J. García: Methodology, Investigation, Formal analysis. **Thomas A. Comerford:** Investigation, Formal analysis. **Carmen Montoro:** Investigation, Formal analysis. **Eli Zysman-Colman:** Writing – review & editing, Supervision, Funding acquisition. **José Alemán:** Writing – review & editing, Writing – original draft, Supervision, Funding acquisition, Conceptualization. **Silvia Cabrera:** Writing – review & editing, Writing – original draft, Supervision, Funding acquisition, Conceptualization.

Declaration of competing interest

The authors declare the following financial interests/personal relationships which may be considered as potential competing interests: [Montaña J García reports financial support was provided by Spanish Government. If there are other authors, they declare that they have no known competing financial interests or personal relationships that could have appeared to influence the work reported in this paper.].

Data availability

All the data is available in the supporting information file. The research data supporting this publication can be accessed at https://doi.org/10.17630/a7067987-5a76-4a70-83c1-f49ed9506d31.

Acknowledgments

Financial support was provided by the Spanish Government (PID2021-122299NB-100, TED2021-129999B-C32, TED2021-130470B-100), "Comunidad de Madrid", and European Structural Funds (S2018/NMT-4367), "Proyectos Sinérgicos I + D (Y2020/NMT-6469) and "Comunidad de Madrid" (SI1/PJI/2019-00237). M. J. G. thanks Spanish Government for her FPI predoctoral fellowship (PRE2019-090203). EZ-C thanks the Engineering and Physical Sciences Research Council (EP/W015137/1, EP/W007517/1).

Appendix A. Supplementary material

Supplementary data to this article can be found online at https://doi.org/10.1016/j.jcat.2024.115368.

References

[1] a) Y. Yan, J. Miao, Z. Yang, F.-X. Xiao, H. B. Yang, B. Liu, Y. Yang, Carbon Nanotube Catalysts: Recent Advances in Synthesis, Characterization and Applications. Chem. Soc. Rev. 44 (2015) 3295-3346. b) G. Bottari, G. de la Torre, D. T. Guldi, T. Torres, Covalent and Noncovalent Phthalocyanine–Carbon Nanostructure Systems: Synthesis, Photoinduced Electron Transfer, and Application to Molecular Photovoltaics. Chem. Rev. 110 (2010) 6768-6816. c) M. Zhao, Y. Wu, J.-P. Cao, Carbon-Based Material-Supported Palladium Nanocatalysts in Coupling Reactions: Discussion on their Stability and Heterogeneity. App. Organomet. Chem. 34 (2020) e5539. d) M. Blanco, S. Cembellín, S. Agnoli, J. Alemán, Ruthenium-*p*-cymene Complex Side-Wall Covalently Bonded to Carbon Nanotubes as Efficient Hybrid Transfer Hydrogenation Catalyst. ChemCatChem 13 (2021) 5156-5165.

[2] a) R. K. Sharma, P. Yadav, M. Yadav, R. Gupta, P. Rana, A. Srivastava, R. Zboril, R. S. Varma, M. Antonietti, M. B. Gawande, Recent development of covalent organic frameworks (COFs): synthesis and catalytic (organic-electro-photo) applications. Mater. Horiz. 7 (2020) 411-454. b) D. Chakraborty, D. Mullangi, C. Chandran, R. Vaidhyanathan, Nanopores of a Covalent Organic Framework: A Customizable Vessel for Organocatalysis. ACS Omega 18 (2022) 15275-15295. c) H. Salemi, M. Debruyne, V. Van Speybroeck, P. Van Der Voort, M. D'hooghe, C. V. Stevens, Covalent organic framework supported palladium catalysts. J. Mater. Chem. A 10 (2022) 20707-20729. d) C.-L. Zhang, T. Zhou, Y.-Q. Li, X. Lu, Y.-B. Guan, Y.-C. Cao, G.-P. Cao, Microenvironment Modulation of Metal-Organic Frameworks (MOFs) for Coordination Olefin Oligomerization and (co)Polymerization. Small 19 (2023) 2205898.

[3] a) A. Perazio, G. Lowe, R. Gobetto, J. Bonin, M. Robert, Light-driven catalytic conversion of CO_2 with heterogenized molecular catalysts based on fourth period transition metals. Coord. Chem. Rev. 443 (2021) 214018. b) N. Pal, D. Chakraborty, E.-B. Cho, J. G. Seo, Recent Developments on the Catalytic and Biosensing Applications of Porous Nanomaterials. Nanomaterials 13 (2023) 2184. c) S. Freeburne, B. Hunter, K. Bell, C. W. Pester, Heterogeneous Photocatalysts for Light-Mediated Reversible Deactivation Radical Polymerization. ChemPhotoChem (2023) e202300090.

[4] a) T. Kitanosono, K. Masuda, P. Xu, S. Kobayashi, Catalytic Organic Reactions in Water toward Sustainable Society. Chem. Rev. 118 (2018) 679-749. b) J. He, C. Janáky, Recent Advances in Solar-Driven Carbon Dioxide Conversion: Expectations versus Reality. ACS Energy Lett. 5 (2020) 1996-2014. c) Y. Zhao, Z. Niu, J. Zhao, L. Xue, X. Fu, J. Long, Recent Advancements in Photoelectrochemical Water Splitting for Hydrogen Production. Electrochem. Energy Rev. 6 (2023) 14.

[5] a) G. Li, B. Wang, D. E. Resasco, Water-Mediated Heterogeneously Catalyzed Reactions. ACS Catal. 10 (2020) 1294–1309. b) K. Stanciakova, B. M. Weckhuysen, Water-active site interactions in zeolites and their relevance in catalysis. Trends in Chem. 3 (2021) 456-468.

[6] a) J. M. R. Narayanam, C. R. J. Stephenson, Visible light photoredox catalysis: applications in organic synthesis. Chem. Soc. Rev. 40 (2011) 102-113. b) C. K. Prier, D. A. Rankic, D. W. C. MacMillan. Visible Light Photoredox Catalysis with Transition Metal Complexes: Applications in Organic Synthesis. Chem. Rev. 113 (2013) 5322-5363. c) N. A. Romero, D. A. Nicewicz, Organic Photoredox Catalysis. Chem. Rev. 116 (2016) 10075-10166. d) K. L. Skubi, T. R. Blu, T. P. Yoon, Dual Catalysis Strategies in Photochemical Synthesis. Chem. Rev. 116 (2016) 10035-10074. e) T. Rigotti, J. Alemán, Visible light photocatalysis – from racemic to asymmetric activation strategies. Chem. Commun. 56 (2020) 11169-11190.

[7] C. Russo, F. Brunelli, G.C. Tron, M. Giustiniano, Visible-Light Photoredox Catalysis in Water, J. Org. Chem. 88 (2023) 6284–6293.

[8] a) F. Hoffmann, M. Cornelius, J. Morell, M. Fröba, Silica-based mesoporous organic-inorganic hybrid materials. Angew. Chem. Int. Ed. 45 (2006) 3216-3251. b) C. Perego, R. Millini, Porous materials in catalysis: challenges for mesoporous materials. Chem. Soc. Rev. 42 (2013) 3956-3976. c) N. Pal, A. Bhaumik, Mesoporous materials: versatile supports in heterogeneous catalysis for liquid phase catalytic transformations. RSC Adv. 5 (2015) 24363-24391. d) T. Cheng, Q. Zhao, D. Zhang, G. Liu, Transition-metal-functionalized ordered mesoporous silicas: an overview of sustainable chiral catalysts for enantioselective transformations. Green Chem. 17 (2015) 2100-2122. e) B. Singh, J. Na, M. Konarova, T. Wakihara, Y. Yamauchi, C. Salomon, M. B. Gawande, Functional Mesoporous Silica Nanomaterials for Catalysis and Environmental Applications. Bull. Chem. Soc. Jpn. 93 (2020) 1459-1496.

[9] a) X. Qian, K. Fuku, Y. Kuwahara, T. Kamegawa, K. Mori, H. Yamashita, Design and Functionalization of Photocatalytic Systems within Mesoporous Silica. ChemSusChem 7 (2014) 1528-1536.

[10] a) J. M. Muñoz-Molina, T. R. Belderrain, P. J. Pérez, Atom Transfer Radical Reactions as a Tool for Olefin Functionalization – On the Way to Practical Applications. Eur. J. Inorg. Chem. (2011) 3155-3164. b) S. Soly, B. Mistry, CN Murthy, Photo-mediated metal-free atom transfer radical polymerization: recent advances in organocatalysts and perfection towards polymer synthesis. Polym. Int. 71 (2022) 159-168.

[11] D.H.R. Barton, M.A. Csiba, J. Cs, Jaszberenyi, Ru(bpy)32+-mediated addition of Se-phenyl p-tolueneselenosulfonate to electron rich olefins, Tetrahedron Lett. 35 (1994) 2869–2872.

[12] C.-J. Wallentin, J.D. Nguyen, P. Finkbeiner, C.R.J. Stephenson, Visible Light-Mediated Atom Transfer Radical Addition via Oxidative and Reductive Quenching of Photocatalysts, J. Am. Chem. Soc. 134 (2012) 8875–8884.

[13] a) O. V. Fedorov, S. I. Scherbinina, V. V. Levin, A. D. Dilman, Light-Mediated Dual Phosphine-/Copper-Catalyzed Atom Transfer Radical Addition Reaction. J. Org. Chem. 84 (2019) 11068-11079. b) B. M. Hockin, C. Li, N. Robertson, E. Zysman-Colman, Photoredox catalysts based on earth-abundant metal complexes. Catal. Sci. Technol. 9 (2019) 889-915. c) S. Engl, O. Reiser, Copper-photocatalyzed ATRA reactions: concepts, applications, and opportunities. Chem. Soc. Rev. 51 (2022) 5287-5299.

[14] E.H. Discekici, N.J. Treat, S.O. Poelma, K.M. Mattson, Z.M. Hudson, Y. Luo, C. J. Hawker, J. Read de Alaniz, A highly reducing metal-free photoredox catalyst: design and application in radical dehalogenations, Chem. Commun. 51 (2015) 11705–11708.

[15] D. González-Muñoz, A. Casado-Sánchez, I. del Hierro, S. Gómez-Ruiz, S. Cabrera, J. Alemán, Size-selective mesoporous silica-based Pt (II) complex as efficient and reusable photocatalytic material, J. Catal. 373 (2019) 374–383.

[16] Y. Zhao, B. Trewyn, I. Slowing, V. Lim, Mesoporous Silica Nanoparticle-Based Double Drug Delivery System for Glucose-Responsive Controlled Release of Insulin and Cyclic AMP, J. Am. Chem. Soc. 131 (2009) 8398–8400.

[17] D. Zhao, Q. Huo, J. Feng, B. Chmelka, G. Stucky, Nonionic Triblock and Star Diblock Copolymer and Oligomeric Surfactant Syntheses of Highly Ordered, Hydrothermally Stable, Mesoporous Silica Structures, J. Am. Chem. Soc. 120 (1998) 6024–6036.

[18] R. Kotcherlakota, A.K. Barui, S. Prashar, M. Fajardo, D. Briones, A. Rodríguez-Diéguez, C.R. Patra, S. Gómez-Ruiz, Curcumin loaded mesoporous silica: an effective drug delivery system for cancer treatment, Biomater. Sci. 4 (2016) 448–459.

[19] a) Y. S. Park, J. Choi, D. Kim, B. Lee, H. Suh, J. H. Kim, Synthesis, Optical, and Electroluminescent Properties of Alternating Copolymer Based on Phenothiazine and Fluorene with Oxadiazole Pendant. Mol. Cryst. Liq. Cryst. 550 (2011) 294–303. b) J. Yang, Z. Ren, B. Chen, M. Fang, Z. Zhao, B. Z. Tang, Q. Peng, Z. Li, Three polymorphs of one luminogen: how the molecular packing affects the RTP and AIE properties? J. Mater. Chem. C, 5 (2017) 9242-9246.

[20] D. González-Muñoz, A. Gómez-Avilés, C.B. Molina, J. Bedia, C. Belver, J. Alemán, S. Cabrera, Anchoring of 10-phenylphenothiazine to mesoporous silica materials: A water compatible organic photocatalyst for the degradation of pollutants, J. Mater. Sci. Technol. 103 (2022) 134–143.

[21] J. Tauc, Adsorption Edge and internal electric fields in amorphous semiconductors, Mater. Res. Bull. 5 (1970) 721–729.

[22] M. Thommes, K. Kaneko, A. Neimark, J.P. Olivier, F. Rodriguez-Reinoso, J. Rouquerol, K.S.W. Sing, Physisorption of gases, with special reference to the evaluation of surface area and pore size distribution, Pure Appl. Chem. 87 (2015) 1051–1069.

[23] M. Kruk, M. Jaroniec, Gas Adsorption Characterization of Ordered Organic–Inorganic Nanocomposite Materials, Chem. Mater. 13 (2001) 3169–3183.

[24] a) D. Díaz-García, P. R. Ardiles, S. Prashar, A. Rodríguez-Diéguez, P. L. Páez, S. Gómez-Ruiz, Preparation and Study of the Antibacterial Applications and Oxidative Stress Induction of Copper Maleamate-Functionalized Mesoporous Silica Nanoparticles. Pharmaceutics 11 (2019) 30. b) D. Díaz-García, L. Sommerova, A. Martisova, H. Skoupilova, S. Prashar, T. Vaculovic, V. Kanicky, I. del Hierro, R. Hrstka, S. Gómez-Ruiz, Mesoporous silica nanoparticles functionalized with a dialkoxide diorganotin(IV) compound: In search of more selective systems against cancer cells. Microporous Mesoporous Mater. 300 (2020) 110154.

[25] F. Khan, R. Misra, Recent advances in the development of phenothiazine and its fluorescent derivatives for optoelectronic applications, J. Mater. Chem. C 11 (2023) 2786–2825.

[26] a) E. Duda, D. Hall, S. Bagnich, C. L. Carpenter-Warren, R. Saxena, M. Y. Wong, D. B. Cordes, A. M. Z. Slawin, D. Beljonne, Y. Olivier, E. Zysman-Colman, A. Köhler, Enhancing Thermally Activated Delayed Fluorescence by Fine-Tuning the Dendron Donor Strength. J. Phys. Chem. B 126 (2022) 552–562. b) A. Kumar Gupta, T. Matulaitis, D. B. Cordes, A. M. Z. Slawin, I. D.W. Samuel, E. Zysman-Colman, Highly twisted α-diketone-based thermally activated delayed fluorescence emitters and their use in organic light-emitting diodes. Can. J. Chem. 100 (2022) 224-233.

[27] We also tested the reaction under **MSN-AP-PTH** using 2 equiv. of LiBr and the yield decreases to 45%, similar to the findings showed in Table 2 for **SBA-15-AP-PTH.**

[28] K. Yu, Z. Gu, R. Ji, L.-L. Lou, F. Ding, C. Zhang, S. Liu, Effect of pore size on the performance of mesoporous materials supported chiral Mn(III) salen complex for the epoxidation of unfunctionalized olefins, J. of Catal. 252 (2007) 312–320.

[29] a) H. Miura, S. Kameyama, D. Komori, T. Shishido, Quantitative Evaluation of the Effect of the Hydrophobicity of the Environment Surrounding Brønsted Acid Sites on Their Catalytic Activity for the Hydrolysis of Organic Molecules. J. Am. Chem.

Soc. 141 (2019) 1636-1645. b) Y. Shiraishi, Y. Sugano, D. Inoue, T. Hirai, Effect of substrate polarity on photocatalytic activity of titanium dioxide particles embedded in mesoporous silica. J. Catal. 264 (2009), 175-182.

[30] In addition, we also tested alkenes **1a-e** using **SBA-15-AP-PTH** material and consistently, the catalytic outcomes were always inferior compared to those achieved with **MSN-AP-PTH**.

[31] a) P. Das, S. Ray, P. Bhanja, A. Bhaumik, C. Mukhopadhyay, Serendipitous Observation of Liquid-Phase Size Selectivity inside a Mesoporous Silica Nanoreactor in the Reaction of Chromene with Formic Acid. ChemCatChem 10 (2018) 2260-2270. b) K. Cheng, M. Virginie, V. V. Ordomsky, C. Cordier, P. A. Chernavskii, M. I. Ivantsov, S. Paul, Y. Wang, A. Y. Khodakov, Pore size effects in high-temperature Fischer–Tropsch synthesis over supported iron catalysts. J. Catal. 328 (2015) 139-150.